

either 10 ms before the onset of the EPSP in one cell and 10 ms after the onset of each EPSP in the other cell (Fig. 3, B and C). After this stimulation, the EPSP amplitude in the neuron in which the postsynaptic APs occurred 10 ms before the EPSPs was reduced, whereas it was increased when the postsynaptic AP occurred 10 ms after the onset of the EPSPs (Fig. 3, B and C), which suggests that postsynaptic AP can up- or down-regulate the amplitude of EPSPs, depending on the precise timing of synapse activation.

These observations suggest that the dendritic APs are a trigger for modifications of the functional synaptic connectivity between neocortical pyramidal neurons. The result of synaptic integration, encoded within the back-propagating AP, is conveyed to dendrites, and hence the back-propagating AP could be regarded as a "binding signal" for active synaptic contacts. A single synaptic contact could therefore be modified in the context of the summed activity of all the contacts on the neuron. The finding that EPSPs were up- or down-regulated, depending on the precise timing of EPSPs with respect to APs, further suggests that single synapses are modified according to the temporal relations of the electrical activity of the neurons in a network (14).

#### REFERENCES AND NOTES

1. D. O. Hebb, *The Organization of Behavior* (Wiley, New York, 1949).
2. T. V. P. Bliss and G. L. Collingridge, *Nature* **361**, 31 (1993).
3. M. J. Friedlander, R. J. Sayer, S. J. Redman, *J. Neurosci.* **10**, 814 (1990); R. Malinow, *Science* **252**, 722 (1991); V. Y. Bolshakov and S. A. Siegelbaum, *ibid.* **269**, 1730 (1995); C. Stricker, A. C. Field, S. J. Redman, *J. Physiol.* **490**, 443 (1996).
4. G. Stuart and B. Sakmann, *Nature* **367**, 69 (1994).
5. W. G. Regehr, J. A. Connor, D. W. Tank, *ibid.* **341**, 533 (1989); H. Markram, P. J. Helm, B. Sakmann, *J. Physiol.* **485**, 1 (1995); J. Schiller, F. Helmchen, B. Sakmann, *ibid.* **487**, 583 (1995); F. Helmchen, K. Imoto, B. Sakmann, *Biophys. J.* **70**, 1069 (1996).
6. Slice preparation, electrical recordings using Nomarski optics, and anatomical reconstructions for the localization of synapses were as described (7). Rats (Wistar) aged 14 to 16 days were used because cortical synapses are most plastic at these ages [K. Fox, *Neuron* **15**, 485 (1995)]. Data are presented as the mean  $\pm$  SEM. The significance of changes was determined with independent two-tailed *t* tests (significance,  $P < 0.05$ ).
7. H. Markram, J. Lübke, M. Frotscher, A. Roth, B. Sakmann, *J. Physiol.*, in press.
8. H. Markram and M. Tsodyks [*Nature* **382**, 807 (1996)] showed that the increase caused by pairing of pre- and postsynaptic activity only applies when tested by low-frequency (<5 Hz) stimulation.
9. Passive membrane properties were measured immediately after whole-cell measurements. Control test EPSPs evoked by single presynaptic APs at 0.25 Hz were recorded from 2 to 3 min after whole-cell recording. After a 10- to 12-min control period, the pairing protocol (detailed in the figure legends) was initiated, test EPSPs were recorded for 10 to 15 min, and the passive membrane properties were measured again. Test EPSPs were then continuously re-

- corded for 30 to 60 min. Amplitudes of EPSPs (average of 75) were measured as the difference between onset (5 to 10 ms before) and peak of the EPSP (1 to 2 ms). Pairs in which the control average EPSPs differed by more than 10% were discarded. The maximum deviation from the baseline at any time during a 10- to 50-min period after pairing was used to represent the change in the EPSP. The time axes of all experiments were normalized to the pairing period.
10. B. Gustafsson, H. Wigstrom, W. C. Abraham, Y.-Y. Huang, *J. Neurosci.* **7**, 774 (1987); S. R. Kelso, A. H. Ganong, T. H. Brown, *Proc. Natl. Acad. Sci. U.S.A.* **83**, 5326 (1986). Block of calcium channels by QX-314 could contribute to the lack of effects (M. J. Talbot and R. J. Sayer, *J. Neurophysiol.* **70**, 2120 (1996)).

11. The conduction velocity in thin basal dendrites is estimated to be roughly 0.2 m/s [estimated from (4)] and the back-propagating AP would thus reach most synapses within 1 ms.
12. D(-)-2-Amino-5-phosphonopentanoic acid (50  $\mu$ M) was applied to six connections (2).
13. P. K. Stanton and T. J. Sejnowski, *Nature* **339**, 215 (1989).
14. W. Singer, *Annu. Rev. Physiol.* **55**, 349 (1993).
15. We thank L. Wollmuth, F. Helmchen, G. Borst, D. Feldmeyer, A. Roth, and O. Ohana for their comments on the manuscript and A. Roth for simulations to estimate AP delays in the dendrite. H.M. was supported by a Minerva Fellowship.

4 October 1996; accepted 22 November 1996

## Microtubule Treadmilling in Vivo

Vladimir I. Rodionov and Gary G. Borisy\*

In vivo, cytoplasmic microtubules are nucleated and anchored by their minus ends at the centrosome and are believed to turn over by a mechanism termed dynamic instability: depolymerization and repolymerization at their plus ends. In cytoplasmic fragments of fish melanophores, microtubules were shown to detach from their nucleation site and depolymerize from their minus ends. Free microtubules moved toward the periphery by treadmilling—growth at one end and shortening from the opposite end. Frequent release from nucleation sites may be a general property of centrosomes and permit a minus-end mechanism of microtubule turnover and treadmilling.

Microtubules (MTs) are fibrillar intracellular structures that play important roles in multiple cellular activities, including mitosis, transport, positioning of membrane organelles, and determination of cellular shape. MT arrays within cells are capable of rapid rearrangement that depends to a large extent on MT dynamics—the ability to exchange subunits between the soluble and polymer pools (1). Studies on MT dynamics in vitro demonstrate the existence of two principal mechanisms of subunit exchange known as treadmilling (2) and dynamic instability (3). Treadmilling involves the addition of subunits to one (plus) end of an MT and loss of subunits from the opposite (minus) end. Dynamic instability is defined by gain and loss of subunits at the same end (either plus or minus) of an MT during growth and shortening. In living cells, where the minus ends of MTs are believed to be tightly anchored at the centrosome, MTs are thought to exchange subunits by polymerization and depolymerization at their plus ends, thus using the dynamic instability mechanism (4).

We studied microtubule dynamics in cytoplasmic fragments of fish melanophores, which translocate cytoplasmic pigment granules to the center (aggregation) or to

the periphery (dispersion) along a radial array of MTs (5). Remarkably, melanophore fragments retained the ability to aggregate pigment and organize a radial MT array of correct polarity orientation (with the minus ends at the center) (6) in the apparent absence of the centrosome (7). To study MT dynamics, we fluorescently tagged MTs in melanophores by microinjection of labeled tubulin, microsurgically dissected fragments from the parental cells, and induced pigment aggregation and formation of the MT aster (8). Images of labeled MTs were then sequentially acquired in the living fragments at short time intervals (3 s) for extended periods (10 min) (9).

Playback of the image sequences revealed characteristic patterns of MT behavior. At any given time, about 80% of the MTs ( $n = 1067$ ) appeared to be static, with one end at the pigment aggregate and the other at the plasma membrane. The other 20% of MTs showed dynamic behavior, either primarily growing (10.6%), primarily shortening (9.3%), or moving (~1%) (Fig. 1A). MTs showed only short length excursions at their free ends, as if dynamic instability was suppressed. MTs emerged from the pigment mass and grew toward the periphery (Fig. 1A, MT1), which indicates that the pigment aggregate had the capacity to nucleate MTs. The aggregate also seemed to stochastically release MTs, after which they shortened at their proximal ends (Fig. 1A, MT2). Thus, the two populations of

Laboratory of Molecular Biology, University of Wisconsin, Madison, WI 53706, USA.

\*To whom correspondence should be addressed. E-mail: ggborisy@facstaff.wisc.edu

MTs were interconvertible. Static MTs, after being released from the aggregate, began to shorten; growing MTs, after arriving at the surface, generally became static. In addition to growing and shortening, short MTs of constant length that moved away from the pigment aggregate were observed (Fig. 1A, MT3). This last pattern of MT behavior was so remarkable that it provoked the question of the mechanism of movement.

Movement of MTs could be achieved either by transport (MT-dependent motors bound to a cytoplasmic matrix) or by treadmilling (polymerization at the plus end and depolymerization at the minus end). The rate of a motor-driven process need bear no relation to polymerization or depolymerization kinetics. In contrast, treadmilling is possible only if the rate of MT polymerization at the plus end equals the rate of depolymerization at the minus end. Analysis of MT length kinetics showed that, unlike the process of dynamic instability, growing MTs persisted in the growing phase (93% of the time) (Fig. 1B, MT1) and shortening MTs persisted in the shortening phase (92% of the time) (Fig. 1B, MT2). Persistent growth was always at the distal end, and persistent shortening was always at the proximal end, which is consistent with the identification of distal ends as plus and proximal ends as minus. Analysis of instantaneous growth (or shortening) rates for the MT population showed that the average rate of polymerization ( $v^+ = 4.2 \pm 4.2 \mu\text{m}/\text{min}$ ) was essentially equal to the average rate of depolymerization ( $v^- = 4.4 \pm$

$4.1 \mu\text{m}/\text{min}$ ) (Fig. 2). However, the standard deviation was large, presumably because of residual dynamic instability and variation among cell fragments. Translocating MTs with both ends free provided an opportunity for closer analysis at the level of single MTs (Fig. 1B, MT3). Although MTs in different fragments varied in their absolute rate of movement, the ratio  $v^+/v^-$  for individual MTs was essentially unity ( $0.99 \pm 0.25$ ) (10). Thus, the major condition of treadmilling was satisfied. Although these results strongly suggested a treadmilling mechanism for MT translocation, they did not rigorously exclude transport.

To definitively distinguish between transport and treadmilling mechanisms, a reference mark was placed on translocating MTs by photobleaching a narrow zone with a laser microbeam. If MTs were transported, the zone of bleaching would move with the MT so that the distances between the zone and the ends of the MT would remain constant. Alternatively, if MTs treadmilled, the zone would remain stationary but the distance from the zone to the leading end would increase and the distance to the trailing end would decrease. Bleached zones placed on growing (Fig. 3, A and D) and shortening (Fig. 3, B and E) MTs did not inhibit either growth or shortening and always remained stationary. When a moving MT was irradiated with a laser microbeam ( $n = 6$ ), its leading end advanced away from the photobleached zone, whereas its trailing end approached the zone, ultimately crossing it and appearing on the other side (Fig. 3, C and F), which

demonstrated that MTs moved by a treadmilling mechanism.

Our results permit a characterization of the MT life cycle in melanophore fragments (Fig. 3, G and H). MTs are nucleated at the pigment aggregate and grow radially outward, and their plus ends become stabilized at the plasma membrane. At some point, the minus ends are released from the aggregate and shorten toward the membrane, and the MT disappears (Fig. 3G). If MTs are released from the aggregate before their plus ends reach the plasma membrane, they treadmill to the periphery (Fig. 3H). The model predicts that in the steady state, the number of growing and shortening MTs should be the same, which was in fact observed. The two behavior patterns can be related to each other by postulating a "residence time" for an MT minus end to remain at the aggregate before it is released. Using a simple model (11) and experimental parameters, we calculated the average residence time to be  $43 \pm 16$  min.

Why do melanophore fragments display an opposite-end pattern of MT turnover instead of dynamic instability? In cytoplasmic fragments, the pigment aggregate rather than the centrosome serves as a site for MT nucleation. Presumably, MTs are more weakly attached to pigment granules than to the centrosome and thus have a higher probability of being released. Frequent release, followed by depolymerization of MTs

**Fig. 1.** Microtubule behavior in melanophore fragments (14). **(A)** Live fluorescence images of microtubules in a fragment with pigment granules aggregated to the center. Single panel at left, MT distribution in a fragment at low magnification. Scale bar, 10  $\mu\text{m}$ . Panels at right, time sequence of MTs in the same fragment at higher magnification. MT1 grows at its distal end, MT2 shortens at its proximal end, and MT3 translocates through the cytoplasm from the aggregate to the plasma membrane. MT3 was exceptional in that it failed to stop on arrival at the membrane; rather, it moved along the fragment edge, stopping at the next orthogonal surface. Time in seconds is indicated at the lower left of each panel. **(B)** Change of distance from the pigment aggregate of ends of the three MTs shown in (A).

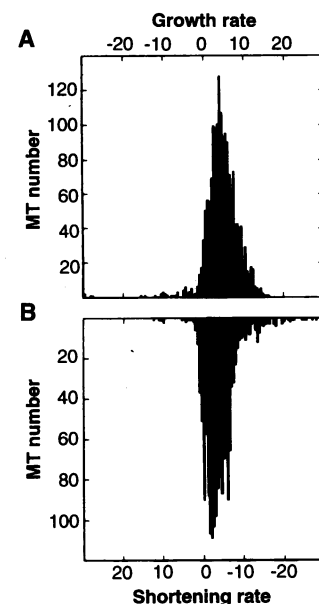
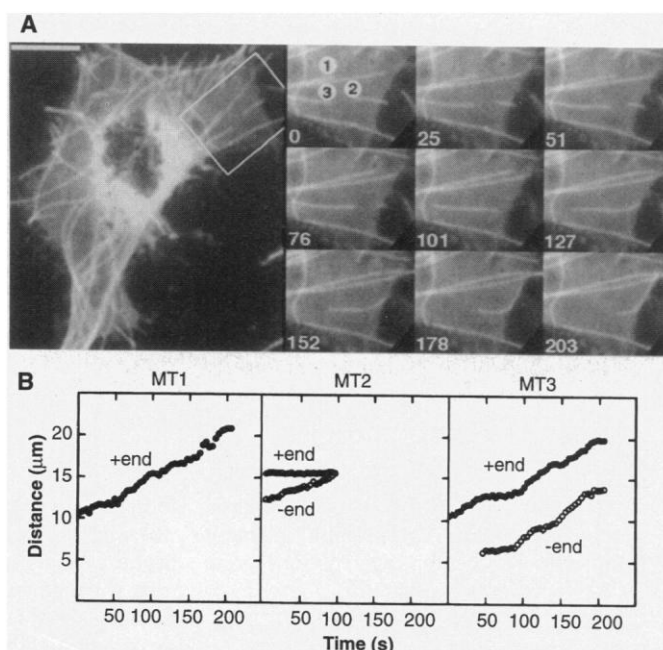


**Fig. 2.** Frequency histograms of rates of MT polymerization at **(A)** the distal (plus) ends and depolymerization at **(B)** the proximal (minus) ends. Change of MT length was quantitated for 47 growing and 45 shortening MTs in 10 fragments. Rates of MT growth or shortening for each time point in the series of images were calculated with a running average of five time points.

at their minus ends, would have the consequence of increasing the steady-state concentration of tubulin monomers. We observed depolymerization rates of 4  $\mu\text{m}/\text{min}$ , which is more than two orders of magnitude faster than the treadmilling reported in vitro (2). At such rates, the predicted increase in tubulin concentration might be sufficient to significantly reduce the frequency of MT catastrophe, suppressing dynamic instability. Thus, decrease in the residence time at the nucleation site may provide a mechanism for switching the pattern of MT turnover.

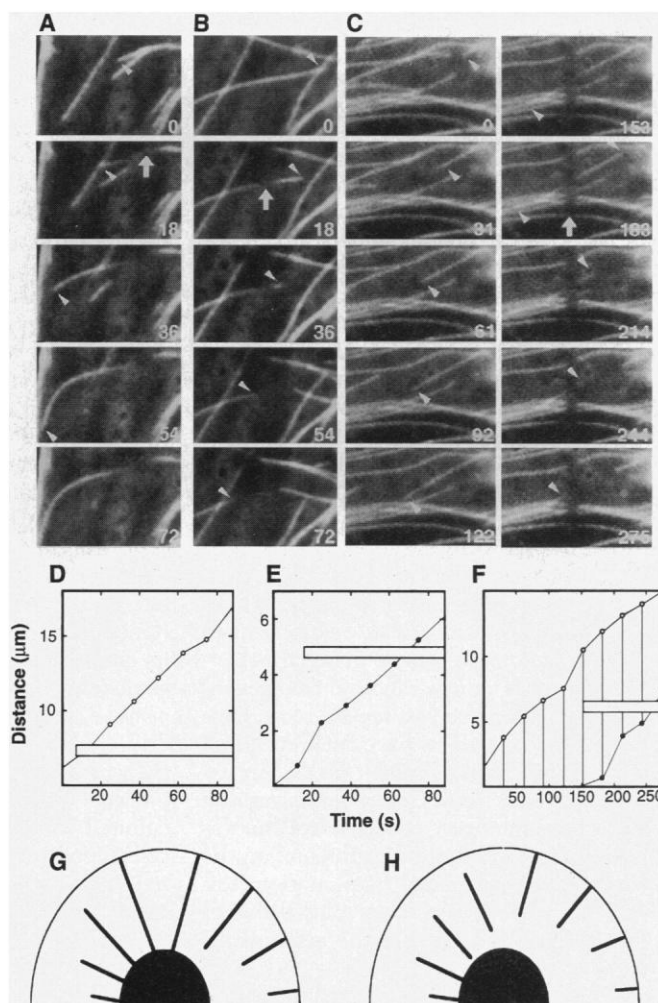
Treadmilling of free MTs does not preclude similar behavior by attached MTs. Tubulin flux or treadmilling has been described for MTs of the mitotic spindle (12). These differ from free MTs in that their ends are anchored at the kinetochore and spindle pole, and their apparent treadmilling has been interpreted to be the result of coupled motor activity (12). In interphase cells, MTs are generally considered to be anchored to the centrosome. However, the literature contains a number of reports suggesting that MTs can be released (13). Our discovery of treadmilling of free MTs in

vivo focuses increased attention on the MT minus end and underscores the importance of understanding how it interacts with the centrosome.

REFERENCES AND NOTES

1. B. J. Soltys and G. G. Borisy, *J. Cell Biol.* **100**, 1682 (1985); E. Schulze and M. Kirschner, *ibid.* **104**, 277 (1986).
2. R. L. Margolis and L. Wilson, *Nature* **293**, 705 (1981).
3. T. J. Mitchison and M. W. Kirschner, *ibid.* **312**, 237 (1984).
4. P. J. Sammak, G. J. Gorbosky, G. G. Borisy, *J. Cell Biol.* **104**, 395 (1987); P. J. Sammak and G. G. Borisy, *Nature* **332**, 724 (1988); E. Schulze and M. Kirschner, *ibid.* **334**, 356 (1988); L. Cassimeris, N. K. Pryer, E. D. Salmon, *J. Cell Biol.* **107**, 2223 (1988).
5. M. Schliwa and U. Euteneuer, *Am. Zool.* **23**, 479 (1983); R. Fujii, *Int. Rev. Cytol.* **143**, 191 (1993); L. H. Haimo and C. D. Thaler, *BioEssays* **16**, 727 (1994).
6. M. McNiven, M. Wang, K. R. Porter, *Cell* **37**, 753 (1984); M. McNiven and K. R. Porter, *J. Cell Biol.* **103**, 1547 (1986); *ibid.* **106**, 1593 (1988).
7. V. I. Rodionov and G. G. Borisy, in preparation.
8. Melanophores of black tetra (*Gymnocorymbus ternetzi*) were cultured on carbon-coated glass cover slips as described previously [F. K. Gyoeva, E. V. Leonova, V. I. Rodionov, V. I. Gelfand, *J. Cell Sci.* **88**, 649 (1987)] and injected with Cy3-labeled porcine brain tubulin prepared as described previously for X-rhodamine-labeled tubulin [P. J. Sammak and G. G. Borisy, *Nature* **332**, 724 (1988)]. Cytoplasmic fragments were dissected from peripheral regions with a glass microneedle, tip diameter  $\sim 0.1 \mu\text{m}$ . Aggregation of pigment granules and formation of a radial MT array were induced by  $10^{-5} \text{ M}$  adrenalin.
9. Cover slips with attached fragments were mounted into sealed Rose chambers filled with culture medium containing 20 mM lactic acid and 2% Oxyrase to remove oxygen. MT images were captured with a charge-coupled device (CCD) camera at 3-s intervals. Acquisition of live fluorescence images of MTs was described in detail previously [V. I. Rodionov, S.-S. Lim, V. I. Gelfand, G. G. Borisy, *J. Cell Biol.* **126**, 1455 (1994)]. Distances were measured with the use of Image-1 (Universal Imaging) software, and data were analyzed in Sigmaplot (Jandel Scientific, San Rafael, CA).
10. Change of position was determined for leading and trailing ends of individual moving MTs. Rates of movement were calculated as five-point running averages as described in the legend to Fig. 2, and the mean velocities were determined. The ratio of the mean velocities  $v^+/v^-$  for individual MTs ( $n = 6$ ) showed less variation than the ratio for averages of populations of MT ends.
11. If  $P_g$  is the fraction of growing MTs,  $P_s$  the fraction of shortening MTs, and  $P_{\text{bec}}$  the fraction of stationary MTs with both ends capped (at the pigment aggregate and at the plasma membrane), then  $P_g + P_s + P_{\text{bec}} = 1$ . Because in the steady state  $P_g = P_s$  and the rate of growth  $v^+$  equals the rate of shortening  $v^-$ ,  $P_{\text{bec}} = 1 - 2P_g = 1 - 2t_g/(\tau + t_s) = 1 - 2(R/v^+)/(\tau + R/v^+)$ , where  $R$  is the radius of a fragment,  $t_g$  is the time required for a MT to grow,  $t_s$  is the time required for an MT to shorten from the aggregate to the plasma membrane, and  $\tau$  is the residence time. The equation solved for  $\tau$  is  $\tau = R/v^+(1 + P_{\text{bec}})/(1 - P_{\text{bec}})$ . A value of  $\tau = 43 \text{ min}$  was calculated for  $R = 20 \mu\text{m}$ , mean velocity  $v^+ = 4 \mu\text{m}/\text{min}$ , and  $P_{\text{bec}} = 0.79$ . Treadmilling MTs would appear if  $\tau < 5 \text{ min}$ . Assuming that residence times are distributed normally, a 1% incidence of treadmilling is consistent with a standard deviation in  $\tau$  of 16 min [(43 min - 5 min)/2.3]. An average residence time of  $43 \pm 16 \text{ min}$  predicts that  $\sim 10\%$  of the time an MT would be growing;  $\sim 10\%$  of the time it would be shortening;  $\sim 80\%$  of the time it would appear static, with one end at the pigment aggregate and the other end at the surface; and  $\sim 1\%$  of the time it would appear to be free and treadmilling, as observed.

**Fig. 3.** Photobleach marking of growing, shortening, and translocating MTs (14). Fluorescently labeled MTs growing (A), shortening (B), and translocating (C) away from the pigment aggregate were crossed with the laser microbeam (vertical arrows; time in seconds is shown at the lower right of each panel). Photobleaching did not affect growth (A) and shortening (B) of MTs. Similarly to the bleached zones placed on growing (A) and shortening (B) MTs, the bleached zone placed on translocating MTs (C) remained stationary while the proximal end of the MT first approached the zone, entered it at 244 s, and appeared on its other side at 275 s. Upward-pointing arrowheads in (A) and (C) indicate distal (growing) ends of MTs; downward-pointing arrowheads in (B) and (C) indicate proximal (shortening) ends. (D through F). Change of distance from reference points of ends of MTs shown in (A) through (C). The length and position of the MTs in (F) are shown by the thin vertical lines.



The positions and duration of the bleached zones are shown as open horizontal bars. (G and H) MT life cycle. (G) Primary pattern of MT turnover. MTs are nucleated at the pigment aggregate (black disk) and grow at their plus (distal) ends toward the surface. Growth is terminated when their distal ends reach the surface; MTs then appear stationary. Eventually, minus (proximal) ends of stationary MTs are released from the aggregate and MTs depolymerize. (H) Secondary pattern of MT turnover. Same as for primary pattern, but MT minus ends release from the pigment aggregate before their plus ends reach the surface. Because the rates of polymerization and depolymerization at the opposite ends of MTs are balanced, they treadmill toward the surface without substantial change in length. The processes involved in both patterns are the same; the only difference is whether release at the minus end follows or precedes arrival of the plus end at the surface. A residence time for the MT minus end at the pigment aggregate may be calculated from experimental parameters (11). For a fragment with a radius of 20  $\mu\text{m}$ , polymerization (or depolymerization) velocities of  $\sim 4 \mu\text{m}/\text{min}$  mean that MTs would grow (or shorten) for 5 min before arriving at the surface (or disappearing). Treadmilling MTs would appear if they were released from the aggregate within 5 min of their nucleation.

12. T. Mitchison, *J. Cell Biol.* **109**, 637 (1989); Y. Zhai, P. J. Kronebusch, G. G. Borisy, *ibid.* **131**, 721 (1995).
13. T. Kitanishi-Yumura and Y. Fukui, *Cell Motil. Cytoskeleton* **6**, 106 (1987); E. McBeath and K. Fujiwara, *Eur. J. Cell Biol.* **52**, 1 (1990); L. D. Belmont, A. A. Hyman, K. E. Sawin, T. J. Mitchison, *Cell* **62**, 579 (1990); F. J. Ahmad and P. W. Baas, *J. Cell Sci.* **108**, 2761 (1995); I. A. Vorobjev and Y. S. Chentsov, *Eur. J. Cell Biol.* **30**, 149 (1983).
14. Video sequences of Figs. 1 and 3, as well as other sequences showing MT motion in melanophore fragments, can be seen at <http://borisy.bocklabs.wisc.edu/>.
15. We thank J. Peloquin for preparation of labeled tubulin. Supported by NIH grant GM25062 to G.G.B. and NSF grant MCB-9418474 to V.I.R.

27 August 1996; accepted 15 November 1996

## Cancer Chemopreventive Activity of Resveratrol, a Natural Product Derived from Grapes

Meishiang Jang, Lining Cai,\* George O. Udeani, Karla V. Slowing, Cathy F. Thomas, Christopher W. W. Beecher, Harry H. S. Fong, Norman R. Farnsworth, A. Douglas Kinghorn, Rajendra G. Mehta, Richard C. Moon, John M. Pezzuto†

Resveratrol, a phytoalexin found in grapes and other food products, was purified and shown to have cancer chemopreventive activity in assays representing three major stages of carcinogenesis. Resveratrol was found to act as an antioxidant and antimutagen and to induce phase II drug-metabolizing enzymes (anti-initiation activity); it mediated anti-inflammatory effects and inhibited cyclooxygenase and hydroperoxidase functions (antipromotion activity); and it induced human promyelocytic leukemia cell differentiation (antipromotion activity). In addition, it inhibited the development of preneoplastic lesions in carcinogen-treated mouse mammary glands in culture and inhibited tumorigenesis in a mouse skin cancer model. These data suggest that resveratrol, a common constituent of the human diet, merits investigation as a potential cancer chemopreventive agent in humans.

Cancer is the largest single cause of death in both men and women, claiming over 6 million lives each year worldwide. Chemoprevention, the prevention of cancer by ingestion of chemical agents that reduce the risk of carcinogenesis (1), is one of the most direct ways to reduce morbidity and mortality. Cancer chemopreventive agents include nonsteroidal anti-inflammatory drugs (NSAIDs) such as indomethacin, aspirin, piroxicam, and sulindac, all of which inhibit cyclooxygenase (COX) (2). This inhibitory activity is relevant to cancer chemoprevention because COX catalyzes the conversion of arachidonic acid to pro-inflammatory substances such as prostaglan-

dins, which can stimulate tumor cell growth and suppress immune surveillance (3). In addition, COX can activate carcinogens to forms that damage genetic material (4).

In searches for new cancer chemopreventive agents over the past several years, hundreds of plant extracts have been evaluated for their potential to inhibit COX. An extract derived from *Cassia quinquangulata* Rich. (Leguminosae), collected in Peru, was identified as a potent inhibitor, and on the basis of bioassay-guided fractionation, resveratrol (3,5,4'-trihydroxy-*trans*-stilbene) (Fig. 1) was identified as the active principle (5).

The process of chemical carcinogenesis can be divided into three general stages, and chemopreventive agents have been categorized according to the stage that they inhibit (6). Resveratrol inhibits cellular events associated with tumor initiation, promotion, and progression. As noted above, the compound was identified on the basis of its ability to inhibit the cyclooxygenase activity of COX-1 (median effective dose  $ED_{50} = 15 \mu\text{M}$ ) (Fig. 2A), and this activity correlates with antitumor promotion. Although its inhibitory activity was less than that of certain NSAIDs, such as

indomethacin ( $ED_{50} = 2.3 \mu\text{M}$ ) (Fig. 2A), it was much greater than that mediated by compounds such as aspirin ( $ED_{50} = 880 \mu\text{M}$ ). Also, unlike indomethacin and most other NSAIDs, resveratrol inhibited the hydroperoxidase activity of COX-1 ( $ED_{50} = 3.7 \mu\text{M}$ ) (Fig. 2B). Resveratrol-mediated inhibition was specific for the cyclooxygenase activity of COX-1 because there was no discernable activity when oxygen uptake was assessed with COX-2 (Fig. 2A), an inducible form of the enzyme associated with responses such as inflammation (7), and inhibition of the hydroperoxidase activity of COX-2 ( $ED_{50} = 85 \mu\text{M}$ ) (Fig. 2B) was greatly reduced relative to the activity observed with COX-1.

On the basis of these results, we investigated the anti-inflammatory activity of resveratrol. In the carrageenan-induced model of inflammation in rats, resveratrol significantly reduced pedal edema both in the acute phase (3 to 7 hours) and in the chronic phase (24 to 144 hours). The edema-suppressing activity of resveratrol was greater than that of phenylbutazone and was similar to that of indomethacin (Fig. 3). Overall, these data demonstrate the potential of resveratrol to inhibit tumor promotion.

Resveratrol was also found to inhibit events associated with tumor initiation. For example, resveratrol inhibited, in a dose-dependent manner, free-radical formation ( $ED_{50} = 27 \mu\text{M}$ ) when human promyelocytic leukemia (HL-60) cells were treated with 12-O-tetradecanoylphorbol-13-acetate (TPA) (8). The compound also functioned as an antimutagen, as illustrated by its dose-dependent inhibition of the mutagenic response induced by treatment of *Salmonella typhimurium* strain TM677 with 7,12-dimethylbenz(a)anthracene (DMBA) ( $ED_{50} = 4 \mu\text{M}$ ) (9). In addition, resveratrol induced quinone reductase activity with cultured mouse hepatoma (Hepa 1c1c7) cells (concentration required to double activity,  $21 \mu\text{M}$ ) (10), which is relevant because phase II enzymes, such as quinone reductase, are capable of metabolically detoxifying carcinogens (11). An identical response profile was observed with cultured BPC1 hepatoma cells (a derivative of Hepa 1c1c7 cells that is incapable of phase I enzyme induction), indicating that resveratrol is a monofunctional inducer.

We also tested the ability of resveratrol to inhibit the progression stage of carcino-

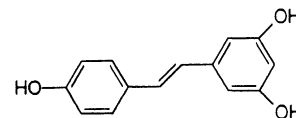


Fig. 1. Structure of resveratrol.

M. Jang, L. Cai, C. W. W. Beecher, H. H. S. Fong, N. R. Farnsworth, A. D. Kinghorn, J. M. Pezzuto, Department of Medicinal Chemistry and Pharmacognosy, College of Pharmacy, University of Illinois at Chicago, Chicago, IL 60612, USA.

G. O. Udeani, Department of Pharmacy Practice, University of Illinois, Chicago, IL 60612, USA.

K. V. Slowing, Departamento de Farmacología, Universidad Complutense de Madrid, 28040 Madrid, Spain.

C. F. Thomas, R. G. Mehta, R. C. Moon, Department of Surgical Oncology, College of Medicine, University of Illinois, Chicago, IL 60612, USA.

\*Present address: Dows Institute for Dental Research, University of Iowa, Iowa City, IA 52242, USA.

†To whom correspondence should be addressed.